Fabricating and Measuring a Cylindrical Mirror for the BigBite Gas Cherenkov (GRINCH) Detector

A thesis submitted in partial fulfillment of the requirements for the degree of Bachelor of Science degree in Physics from the College of William and Mary

by

Colin Cleaves Manning

Advisor: Todd Averett

Senior Research Coordinator: Henry Krakauer

Date: April 2013

Abstract

This paper is a review of the work done to date by the Experimental Nuclear Physics Group at The College of William and Mary in conjunction with Jefferson Lab (JLab) for the BigBite Gas Cherenkov (GRINCH) detector. In additions it will review the history of the experiment, the theory used in the GRINCH detector, and the goals of the project.

I. Introduction

The focus of this project is creating and measuring cylindrical mirrors for the prototype BigBite Gas Cherenkov (GRINCH) detector used in experiment E12-06-122 at Jefferson Lab (JLab). This experiment measures the neutron A_{1n} asymmetry using polarized ^{3}He. Experiment E12-06-122 collides high energy electrons with ^{3}He and measures the scattered electrons at a deflection angle of 30^o. Figure 1 shows the experimental layout of the ^{3}He target and the BigBite spectrometer package.

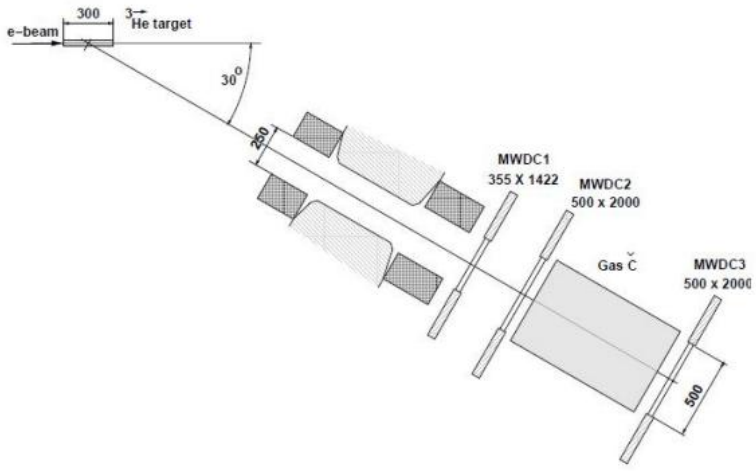

Figure 1: This is a diagram of the BigBite spectrometer and detector. A high energy electron beam is scattered off of a ^{3}He target. The detector lies 30^o from the target axis. The emitted particles go through a dipole magnet, which acts as a momentum selector. Then the particles enter two multi-wire drift chambers for tracking. After the multi-wire drift chambers is a Cherenkov radiation detector, consisting

of a gas chamber and a series of detectors. The particles exit the Cherenkov detector and enter a third multi-wire drift chamber, then into the rest of the sensor array.

The Cherenkov radiation detector acts as a velocity selector which differentiates between pions and electrons. Currently, the Cherenkov radiation detector consists of a gas chamber and a mirror which reflects the Cherenkov radiation onto twenty detectors. These detectors are photomultiplier tubes (PMT's). Photomultiplier tubes convert photons to electrons via the photoelectric effect. Ten of the PMT's are located on the side of the detector that is closest to the initial beam, and the other ten PMT's are located on the opposite side. Figure 2 shows a schematic of the old Cherenkov radiation detector.

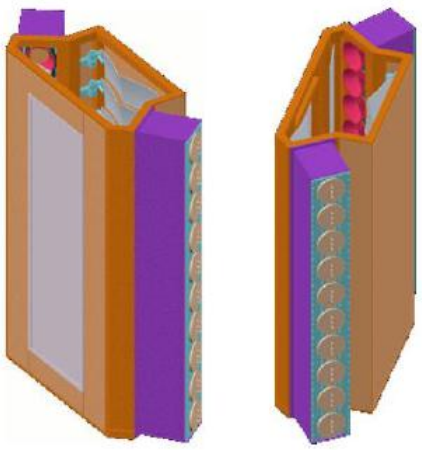

Figure 2: Two views of the BigBite Cherenkov radiation detector. The purple and grey cylinders are ten 5" PMT's, which convert photons emitted by Chernkov radiation into electrons through the photoelectric effect.

The detector currently being used by JLab is being replaced because it was experiencing high levels of background radiation, which were creating false readings for PMT's 1-10 as seen in Figure 3.

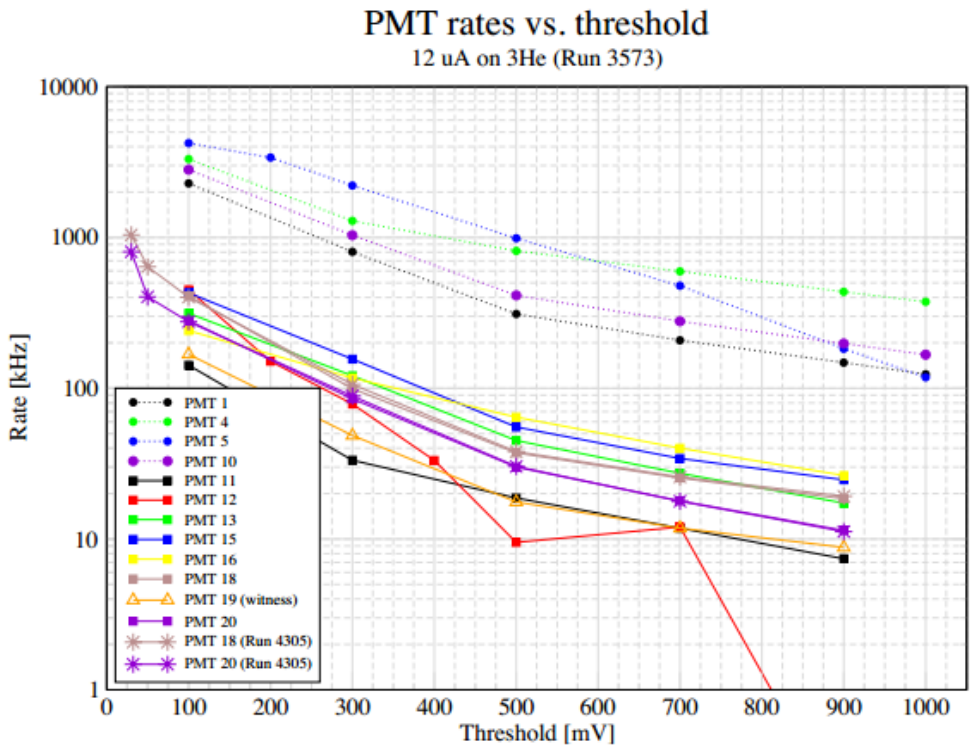

Figure 3: Rates versus discriminator threshold measured in 5" PMT's. PMT 1-10 are on the beam side

Previously the experimental kinematic range was limited by the 6 GeV electron beam. Jlab's upgraded beam energy of 12 GeV will allow A_{n1} to be measured in the deep–inelastic scattering region (DIS), but it will also increase the luminosity by at least a factor of four. The DIS region is where electron scattering is dominated by electron-free quark interactions. GRINCH is designed to have a higher detection rate and lower the rate of false positives created by background radiation. To accomplish this, a ring imaging Cherenkov detector was determined to be the most suitable. To date, a prototype

GRINCH has been designed and built by the William and Mary Physics program using flat mirrors. The next step is to build a cylindrical mirror to focus the Cherenkov radiation onto the PMT's

II. Theory

II.1 Cherenkov Radiation

Cherenkov radiation is caused by a particle traveling faster than the speed of light in a medium, i.e. $v > c/n(\omega)$. Figure 4 depicts the phenomenon of Cherenkov radiation.

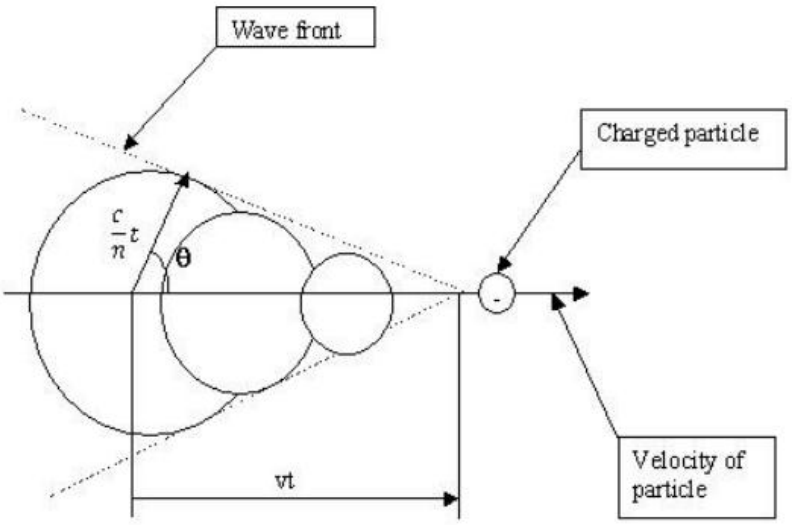

Figure 4: Cherenkov Radiation Front

The radiation is emitted in a cone given by θ_c where:

$$\cos\theta_c = \frac{1}{\beta n(\omega)} = \frac{1}{(v/c)n(\omega)} \quad v = \frac{c}{n} \tag{1}$$

And $\beta = v/c$. The energy radiated through a solid angle $d\Omega$ at a certain frequency ω of light by a particle with charge Ze is given by Equation 2.

$$\frac{d^2E}{d\omega d\Omega} = z^2 \frac{\alpha\hbar}{c} n\beta^2 \sin^2(\theta)\left[\frac{\omega L \sin(\xi(\theta))}{2\pi\beta c\xi(\theta)}\right]^2 \tag{2}$$

L is the thickness of the medium that the particle is traveling through, α is the fine structure constant, n is the refractive index of the medium, and ξ is

$$\xi(\theta) = \frac{\omega L}{2\beta c}(1 - \beta n \cos\theta) \tag{3}$$

Integrating Equation 1 over the solid angle $d\Omega$ yields:

$$-\frac{dE}{d\omega} = z^2 \frac{\alpha\hbar}{c} \omega L sin^2(\theta_c) \tag{4}$$

To obtain the energy per path length, Equation 4 is divided by, then integrated over, frequencies which satisfy the Cherenkov threshold condition ($v > c = n(\omega)$) the velocities that produce Cherenkov radiation (assuming that *L* much larger than the wavelength of the emitted light and *L* is defined as the *x-axis*)

$$-\frac{dE}{dx} = z^2 \frac{\alpha\hbar}{c} \int \omega d\omega \sin^2(\theta_c) = z^2 \frac{\alpha\hbar}{c} \int \omega d\omega \left(1 - \frac{1}{\beta^2 n^2(\omega)}\right) \tag{5}$$

II.2 GRINCH

GRINCH detector stands for **G**as **R**ing-**I**magi**N**g **CH**erenkov detector. It is used as a particle identifier by measuring emitted Cherenkov radiation. The dipole magnets act as a momentum selector. Therefore, all of the particles entering into the GRINCH have the same momentum. This allows us to use relativistic momentum ($p = \gamma m v$) where $\gamma = \frac{1}{\sqrt{1-\frac{v^2}{c^2}}}$. Since pions and electrons have different masses, they will have different velocities but the same momentum. By using an appropriate medium, a threshold velocity can be chosen so that only electrons create Cherenkov radiation.

Figure 1 shows the experimental setup for the entire BigBite apparatus. The GRINCH consists of a vessel filled with C_4F_8O at 1atm and a cylindrical mirror to focus and reflect the Cherenkov

radiation onto a 9X60 PMT array. Figure 5 shows a simulation of the GRINCH apparatus.

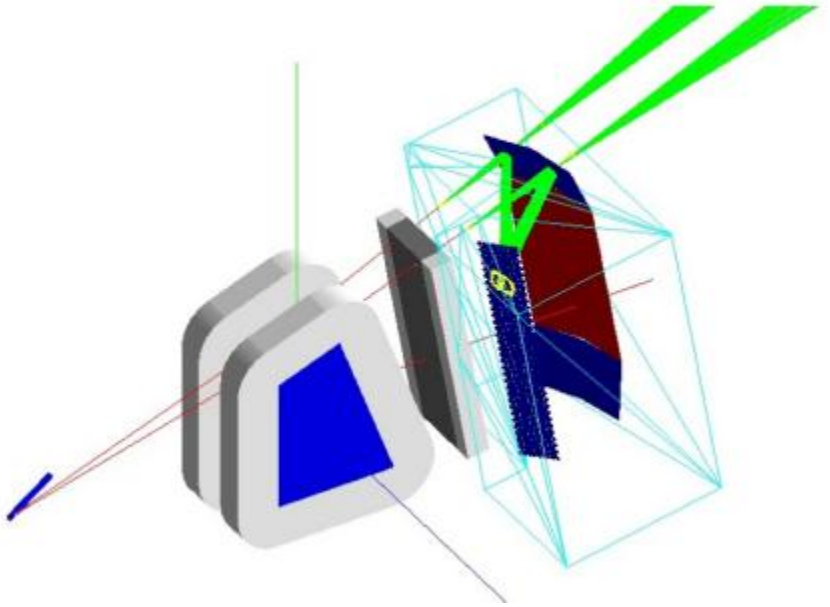

Figure 5: Simulated GRINCH Apparatus. The red lines represent scattered particles. The grey and blue figure is a dipole magnet that acts as a momentum selector. After the dipole magnet is the multi-wire drift chamber, which tracks the particles trajectories. The light blue represent front of the GRINCH. The dark blue is the cylindrical mirror that focuses the Cherenkov radiation onto the PMT's. The green represents Cherenkov radiation which is reflected onto the PMT's, and the yellow represents a simulated target pattern.

Since the radiation is emitted in a cone, this can be used to predict a target pattern on the PMT's (Figure 6).

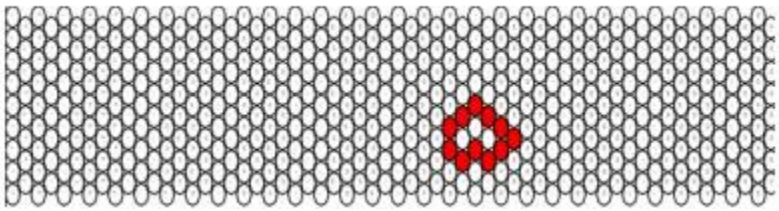

Figure 6: Simulated Cherenkov Radiation event

The 9x60 array of PMT's will be separated by 1mm for magnetic shielding. The PMT's will cover approximately 60% of the total array area. PMT's work by converting photons into electrons via the photoelectric effect. Then a positive voltage is applied in the tube to accelerate the electrons, which create more electrons by colliding with dynodes in the PMT (as seen in Figure 7). The current is measured and analyzed to produce data.

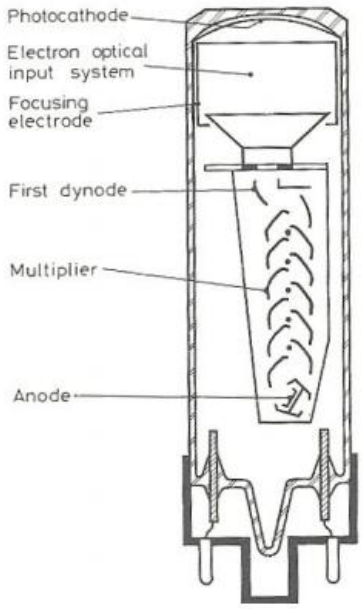

Figure 7: Standard Photomultiplier Tube. The PMT works by photons hitting the photocathode, which emits electrons via the photoelectric effect. The electrons are accelerated towards the anode by an applied electric field. In the path are targets called dynodes, which the electrons impact. Because they were accelerated by the applied electric field, the impact causes the dynode to emit more electrons. This is repeated several times using multiple dynodes. Then the current is analyzed to give data.

III. Current Progress

III.1 Mirror Construction via Stress Induced by a Frame

It was determined that a cylindrical mirror with the dimensions of 72 cm x 42 cm and a radius of curvature of 130 cm was optimal. This project explored two methods of fabricating a mirror with these specifications. The first method was to use a mirror mount to apply stress to a sheet of Lexan, causing it to deform into a curved surface. The mount has several components, which allow us to orient the mirror with several degrees of freedom. The Lexan is inserted directly into two rods. The rods were machined to have a 1/8” slot going down the length of the rod. The rods are connected to the apparatus using two clamps for each side. When the clamps are tightened, the rods do not rotate, but when the clamps are loose, the rods rotate freely. The clamps on each side of the mirror are attached to a plate. The plates can rotate to adjust the pitch of the mirror. Looking at the left side of the mount from the perspective of an incoming laser beam, the plate is mounted to the frame via three bolts. These bolts allow us to increase the stress on the Lexan, which increases the deformation. The whole apparatus is bolted to a square metal frame, which is bolted to the optics table. Figure 8 shows the mirror mount with a flat piece of Lexan, which has been curved by the stress. For purposes of this experiment, *the z-axis* is vertical, the *y-axis* is parallel to the length of the length of the table, and the *x-axis* is parallel to the width of the optics table. The frame of the mount is bolted in the *y-z* plane.

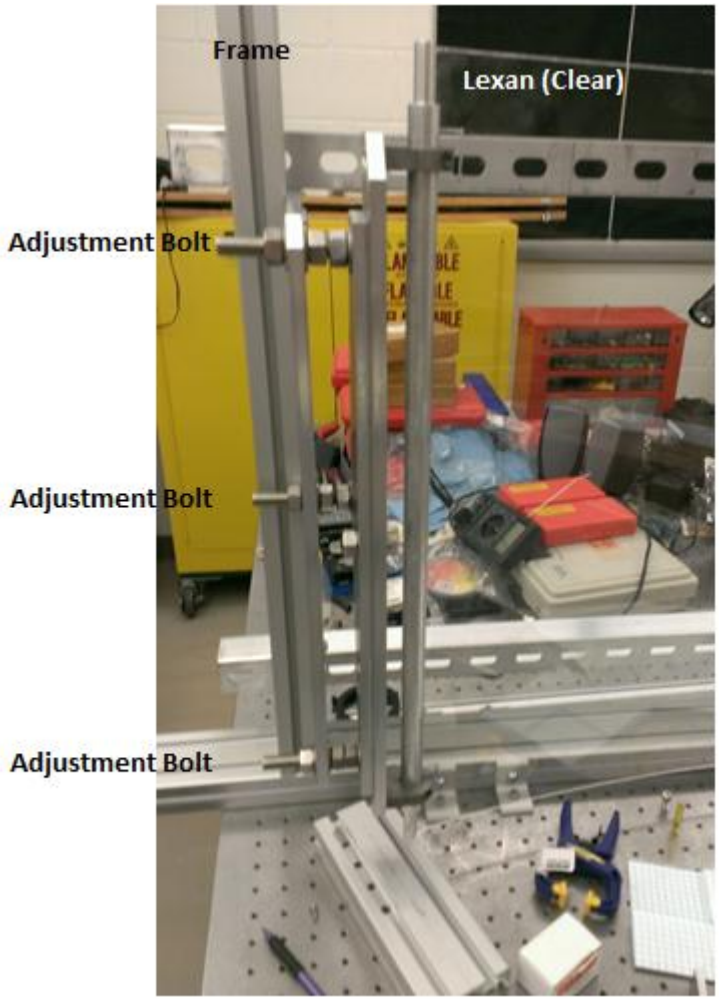

Figure 8: This is a close up of one side of the mirror mount. In this picture the Lexan is inserted into a slot that has been machined down the length of the rod. The two clamps are loose enough to allow the rods to freely rotate in place. The plate that the two clamps are attached to is capable of rotating about the y-axis. The three bolts on the left side of the picture control the chord length of the mirror.

To start we did a mechanical alignment of the mirror. This means that we gave the mirror several characteristics of a circle. The sagittal measurements were taken from the back of the mirror. We mounted two horizontal bars (one near the top of the mirror and one near the bottom) across the back of the frame to use as reference points. We then measured distance from the back of the mirror to the bars at both ends and in the center. This was repeated for the top and bottom of the mirror. A circle with a radius of 130 cm will have an arc length of 86.22 cm and a sagittal length of 7.11 cm was created using the bolts to reduce the distance between the two posts.

III.2 Mirror Measurement

III.2.1.Laser Apparatus

We have built a laser table to measure the radius of curvature by finding the focal length. The laser is on an apparatus that allows us to move the laser forwards, sideways, or rotate in a measured setting (i.e. the movement of the laser can be measured for horizontal, vertical, and rotational movement). The laser is mounted in a metal block attached to two rotating stands. The laser block was fabricated such that the laser sits directly in the center of the two platforms. Figure 9 shows the laser apparatus.

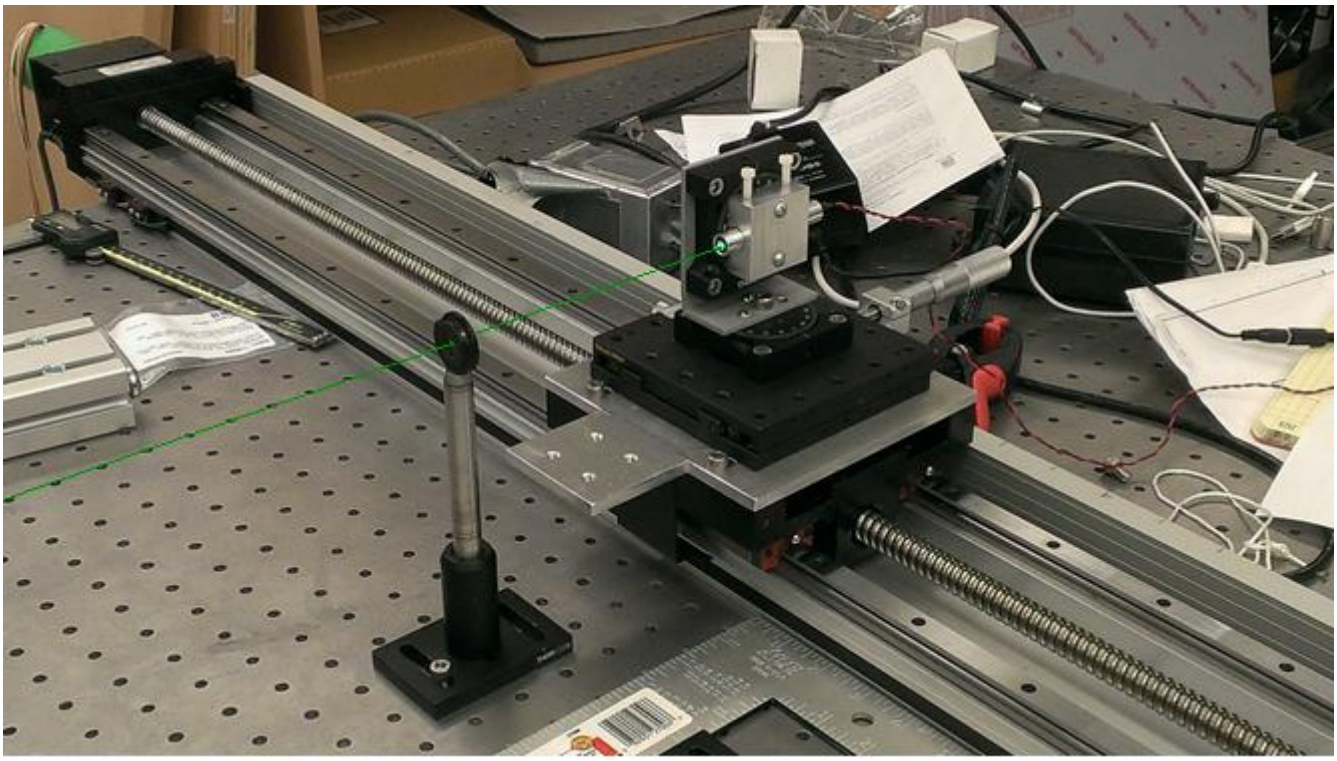

Figure 9: Laser Apparatus. This mounting allows precise control and measurement in the x-y plane and rotation at a given coordinate. The path of the laser has been simulated.

The *y-direction* is defined to be distance from the mirror to the laser track. The *x-direction* is the

movement along the track seen in Figure 9. Once an angle has been set, the rotating stand can be locked to prevent the laser from being disturbed.

III.2.2.Laser Alignment

To minimize degrees of freedom, we decided that the laser and mirror should be oriented to satisfy two criteria; the laser should be parallel to the *x-axis* and the laser beam should reflect back onto itself when it reflects off of the center of the mirror. To satisfy these criteria we used two irises mounted on optical posts. Figure 10 shows the arrangement of the two irises.

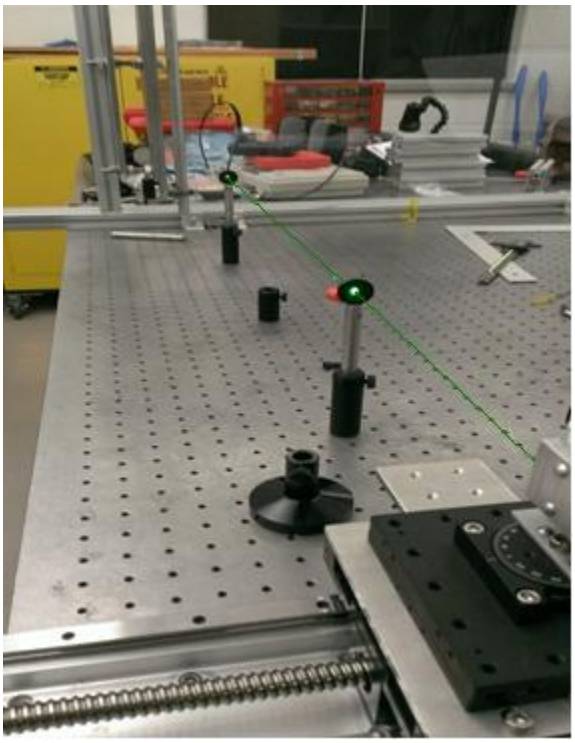

Figure 10: This figure shows the two irises used for alignment in the laser table. The path of the laser beam has been simulated.

The laser was considered to be parallel to the table when the laser passed through both irises when they were almost closed. Figure 11 shows the resulting beam after it passes through the second iris.

Figure 11: This shows the resulting laser beam after it has passed through two nearly closed irises.

To achieve the second criteria we measured the geometric center line of the mirror when it was flat, and marked it. Then we placed the two irises in front of the mark. Then the posts were slightly rotated to move the reflected beam, until it reflected back into the laser. Figure 12 shows the entire setup.

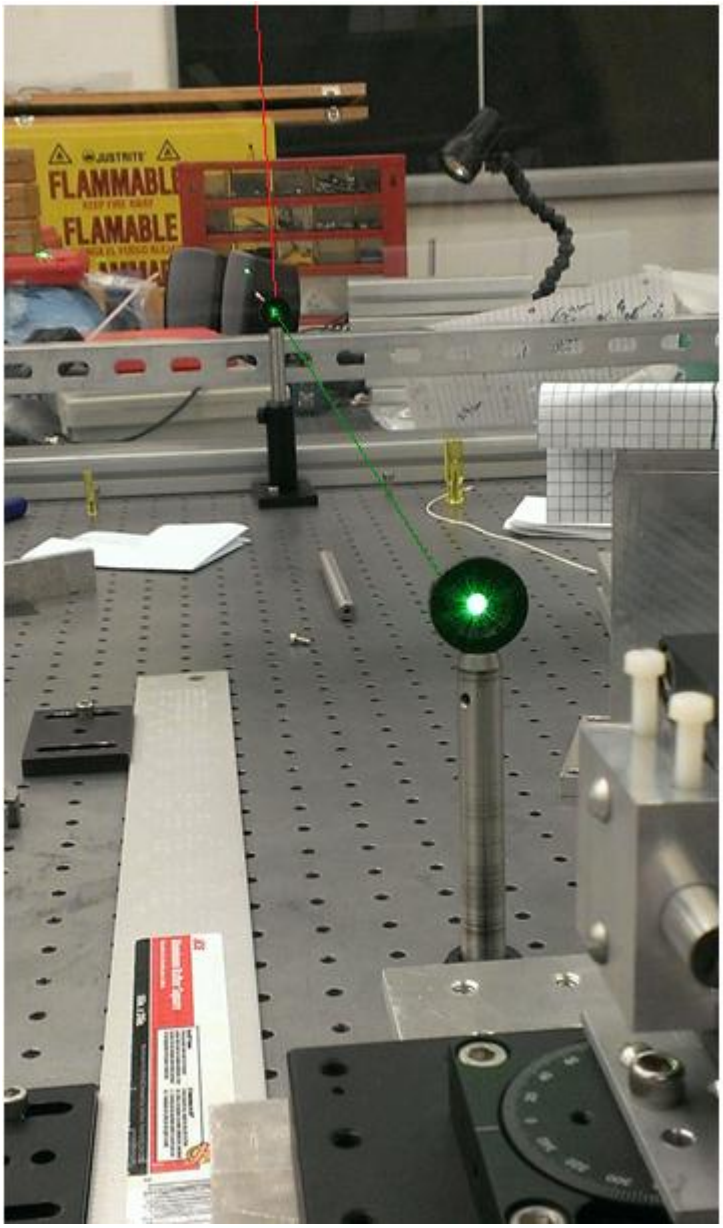

Figure 12: This shows the entire alignment setup. The laser beam(simulated in this image) must pass through both irises and back onto itself to be considered aligned. The center line of the mirror has been highlighted to increase its visibility above the second post.

The laser apparatus was very sensitive to rotational shifts. The laser only needed to be rotated by approximately 1^{o} to have it aligned. Figure 13 shows the alignment angle of the apparatus.

Figure 13: The alignment angle. At this angle the laser will reflect back onto itself when it reflects off of the center of the mirror.

III.2.3.Measuring the Radius of Curvature

To measure the radius of curvature we found the focal point of the mirror. The focal point must be along the line of the laser beam that reflects back onto itself. We created a target with grid lines to track the movement of the reflected beam. We then placed the target in the path of the laser, and marked the line that the laser struck as the center line. The reflected light will only strike this point when the target is at the focal length. Figure 14 shows the target setup.

Figure 14: This shows the set up for the target. The laser is shown striking the back of the target to mark the center line. The center line was continued onto the front of the target. When the laser reflects off of the mirror, the target is moved along the y-axis until the reflected laser strikes the same point on the front of the target.

To find the focal length, the target is moved along the *y-axis* until the reflected laser beam strikes the center line again. This allowed us to make relatively easy measurements of the focal length.

III.2.4.Data Results and Analysis

To make a profile of the mirror, we measured the radius of curvature at several points along the mirror. We panned the laser all the way to the left side of the mirror. The laser's motion in the *x-axis* was controlled by the track that the laser platform was mounted onto. The track moved the platform by a long spiraled rod. The laser was moved by spinning the rod. We then panned the laser to the right by approximately 1 inch (5 rotations of the rod). Data Table 1 shows the resulting focal length measurements and calculated radius of curvatures.

Table 1: This tabulates the measured radius of curvature across the whole mirror. All measurements were taken from the center of the mirror. The region in the center of the mirror has not data, because it was blocked by the target.

Number of turns	Total Inches	Focal Length (cm) ±0 .65 cm	Radius of Curvature (cm) ± 0.65 cm
0	0	81.92	163.83
5	1	81.92	163.83
10	2	82.55	165.10
15	3	83.19	166.37
20	4	83.82	167.64
25	5	83.82	167.64
30	6	83.19	166.37
35	7	83.19	166.37
40	8	81.912	163.83
45	9	80.01	160.02
50	10	76.2	152.4
55	11	76.84	153.67
60	12	76.2	152.4
65	13	74.295	148.59
70	14	No data	No data
75	15	No data	No data
80	16	No data	No data
83	16.6	Back Reflects	No data
85	17	No data	No data
90	18	No data	No data
95	19	No data	No data
97	19.4	77.47	154.94
100	20	77.47	154.94
105	21	77.47	154.94
110	22	77.47	154.94
115	23	77.47	154.94
120	24	78.11	156.21
125	25	78.74	157.48
130	26	79.375	158.75
135	27	80.01	160.02
140	28	81.28	162.56
145	29	81.28	162.56
150	30	82.55	165.1
155	31	83.82	167.64
160	32	84.45	168.91
165	33	85.09	170.18

The average radius of curvature was calculated to be 160.76 ± 0.65 cm. This data suggests that this mirror is not cylindrical, and that doing a mechanical alignment to make the mirror meet the boundary conditions of a cylindrical mirror was not sufficient to create a cylindrical mirror with the correct radius.

To try and reduce the radius of curvature, more curvature was added by twisting the rods holding the mirror in place. This applied more torque to the mirror. This process did make the radius of curvature more constant across more of the mirror, but had the side effect of increasing the radius of curvature. This is due to the fact that the chord length was not decreased, so by artificially curving the mirror, it was forcing the central part of the mirror into a linear shape.

Modeling of the mirror's shape due to stress agrees with the collected data that the radius of curvature will be larger than the desired radius and the curvature will not be constant.

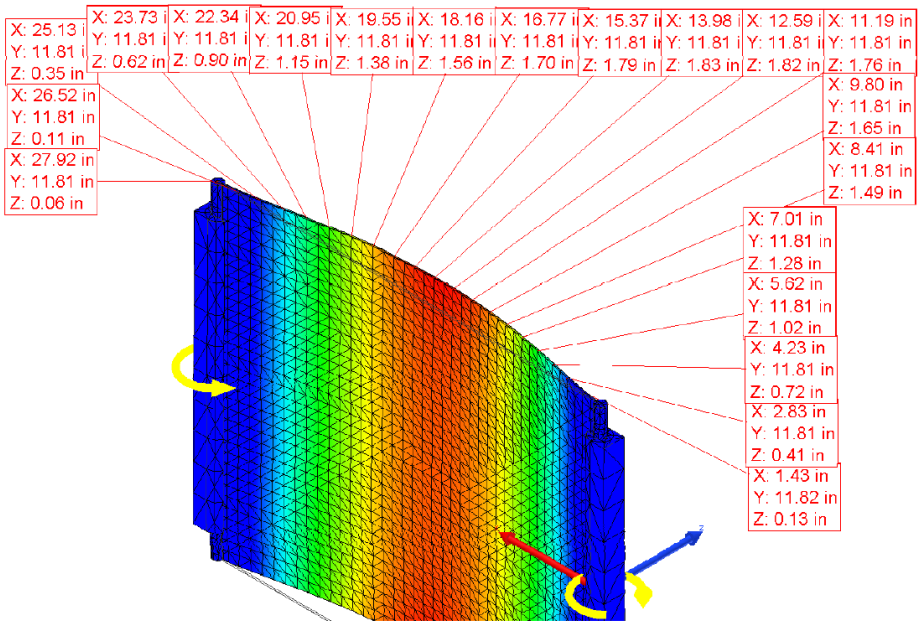

Figure 15: A model of the mirror under constant stress. The color represents the distance from the mirror to the chord.

Analysis of the graph of this model shows that the radius of curvature is not constant throughout the surface. Figure 16 shows that the center region has the smallest radius of curvature of 38.962 in, left outer region has a much larger radius of curvature of 333.9 in, and the right outer region has a radius of curvature of 704.95 in.

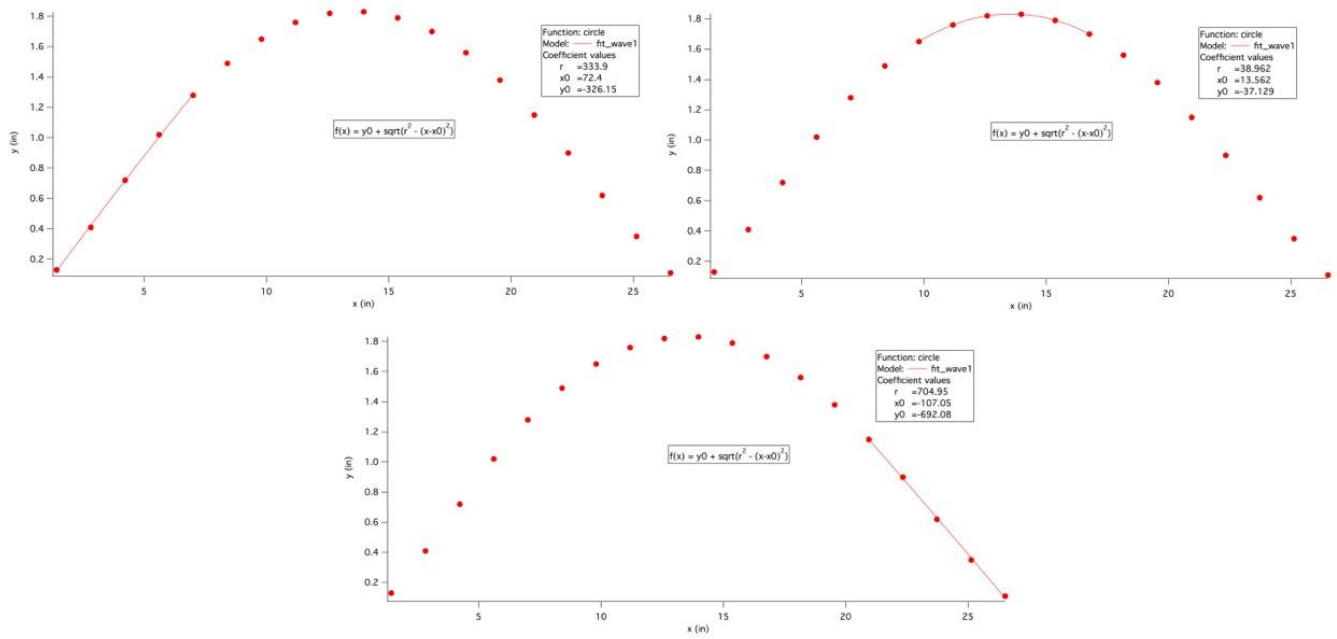

Figure 16: This shows how the model predicts that the radius of curvature will not be constant. The first graph shows the 1st 5 points fitted to a circle, the second graph shows the middle 6 points being fitted to a circle, and the third graph shows the last 5 points being fitted to a circle.

This is due to plate bending theory. For plates that have a ratio of thickness / width < 1/50 von Karman theory is used to model the plate's bending. Von Karman bending is characterized by geometricaly nonlinear bending with membrane deformation. Equation 6 and Equation 7 give the nonlinear set of partial differential equations for von Karman theory.

$$\frac{Eh^3}{12(1-\nu^2)}\nabla^4 W(x,y) - \frac{h\partial}{\partial\chi_\beta}\left(\sigma_{\alpha\beta}\frac{\partial W(x,y)}{\partial\chi_\alpha}\right) = P(x,y) \tag{6}$$

$$\frac{\partial\sigma_{\alpha\beta}}{\partial\chi_\beta} = 0 \tag{7}$$

Where E is Young's modulus, $\sigma_{\alpha\beta}$ is the stress tensor, h is the thickness of the plate, W is the out of plane deflection, $\upsilon = -\frac{d\varepsilon_{trans}}{d\varepsilon_{axial}}$ where ε is the axial or transverse strain, P is the external normal force per area of the plate, $\chi_{a,b}$ is the Airy stress function, and ∇^4 is the biharmonic differential opperator. The biharmonic differential opperator is $\nabla^2\nabla^2$.

$$\nabla^4 W(x,y) = \frac{\partial^4 W}{\partial x^4} + 2\frac{\partial^4 W}{\partial x^4 \partial y^4} + \frac{\partial^4 W}{\partial y^4} \quad (9)$$

In the case where there is no axial, shear, or torsional forces Equation 6 simplifies to Equation 8:

$$\nabla^4 W(x,y) = \frac{12P_o(x,y)*(1-\nu^2)}{Eh^3} \quad (10)$$

If the plate were horizontal, this would require that the plate is supported only around the edges and a downward force is applied. There are two means of supporting the plate. Simply supported is the case where the plate rests on a frame and is free to bend. This scenario is shortened to SSSS, when all four sides of the plate are simply supported. The boundary conditions for SSSS are:

$W(0,y) = 0,\ W(a,y) = 0,\ W(x,0) = 0,\ W(x,b) = 0,\ \frac{\partial^2 W(0,y)}{\partial x^2} = 0,\ \frac{\partial^2 W(a,y)}{\partial x^2} = 0,\ \frac{\partial^2 W(x,0)}{\partial y^2} = 0,\ \frac{\partial^2 W(x,b)}{\partial y^2} = 0.$

Where *a* and *b* are the width and height of the plate respectively. These conditions force the plate to have a deflection of 0 at the edges of the plate, and that the slope is not changing around the edges. The second way of supporting the plate is by clamping the edges. If all four sides are clamped then this is abbreviated as CCCC. The boundary conditions for CCC are:

$W(0,y) = 0,\ W(a,y) = 0,\ W(x,0) = 0,\ W(x,b) = 0,\ \frac{\partial W(0,y)}{\partial x} = 0,\ \frac{\partial W(a,y)}{\partial x} = 0,\ \frac{\partial W(x,0)}{\partial y} = 0,\ \frac{\partial W(x,b)}{\partial y} = 0$

This also forces the edges of the plate to have no deflection (because the slope is 0). However the slope must change in a bent plate, because the slope cannot be 0 everywhere for a curved plate. This entails that the CCCC deflection cannot form a hemispere which has a constant slope.Our setup has two sides clamped and two sides free. This means that our setup cannot form a cylindrical surface.

III.3 Mirror Construction via Heat Deflection

The other method for constructing a cylindrical mirror was to deflect Lexan onto a premade mould. The mould consists of a top half and a bottom half. Each half is comprised of four 0.75" aluminum ribs that were machined to have a radius of curvature of 130 cm. Then a 1/16" sheet of aluminum was epoxied onto the curved surface. Each half of the mould is heated using 4 elecrical heaters glued onto the reverse side of the aluminum sheet. Ten thermocouples were used to monitor the

heating process to ensure even heating. Two heaters were plugged into an electrical surge protector, which was connected to a Variac. A total of 4 Variacs were used; 2 for the top half and 2 for the bottom half. Figure 17 shows the mould.

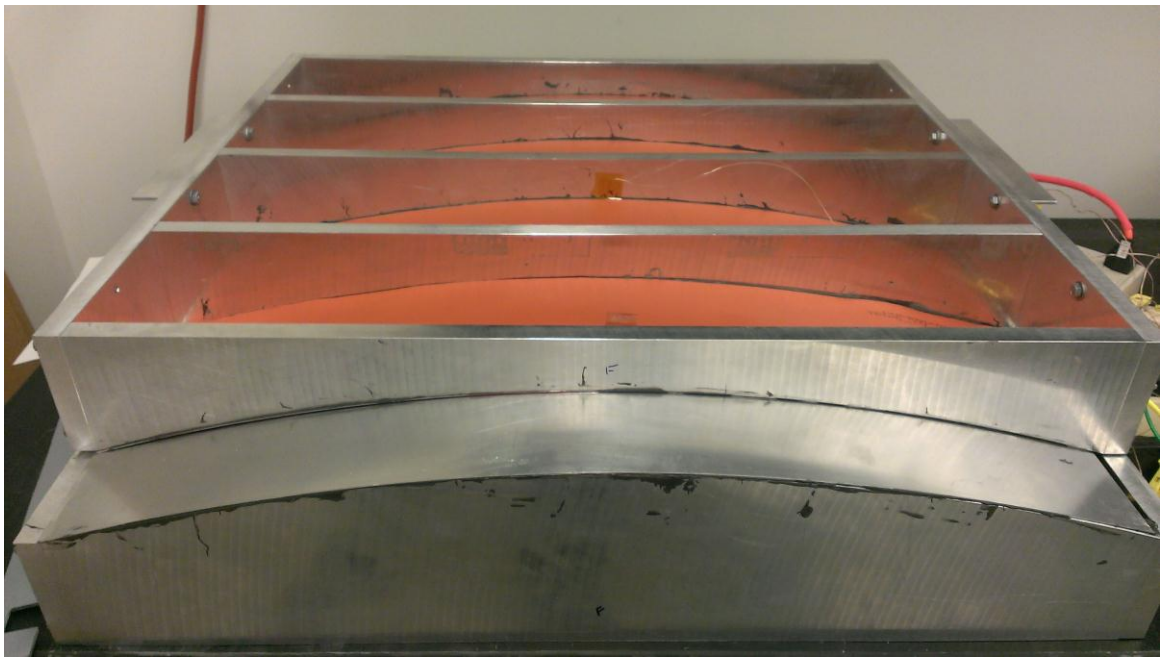

Figure 17: This is the mould used to deform Lexan. It is made of 0.75"aluminum. The orange strips between the struts are the electric heaters. There are 5 thermocouples arranged under the electric heaters to measure the temperature. The underside of the bottom half has a similar setup.

The procedure for slumping Lexan is to place the piece inside the mould between the two halves. It is important to make sure the piece runs parallel to the length of the mould. Then the temperature is slowly raised over the period of 30-40 minutes. This ensures that the mould does not get too hot. Lexan has a deformation temperature of approximately 140^{o}C. This apparatus has been able to achieve temperatures greater than 180^{o}C. Then when the temperature reaches 140^{o} C the heaters are turned off and the apparatus is allowed to cool overnight. This procedure has worked for clear Lexan, mirrored Lexan and polycarbonate honeycomb, although the mirrored Lexan required a lower maximum temperature so that the mirror finish isn't tarnished. Figure 18 shows all three pieces set on each other.

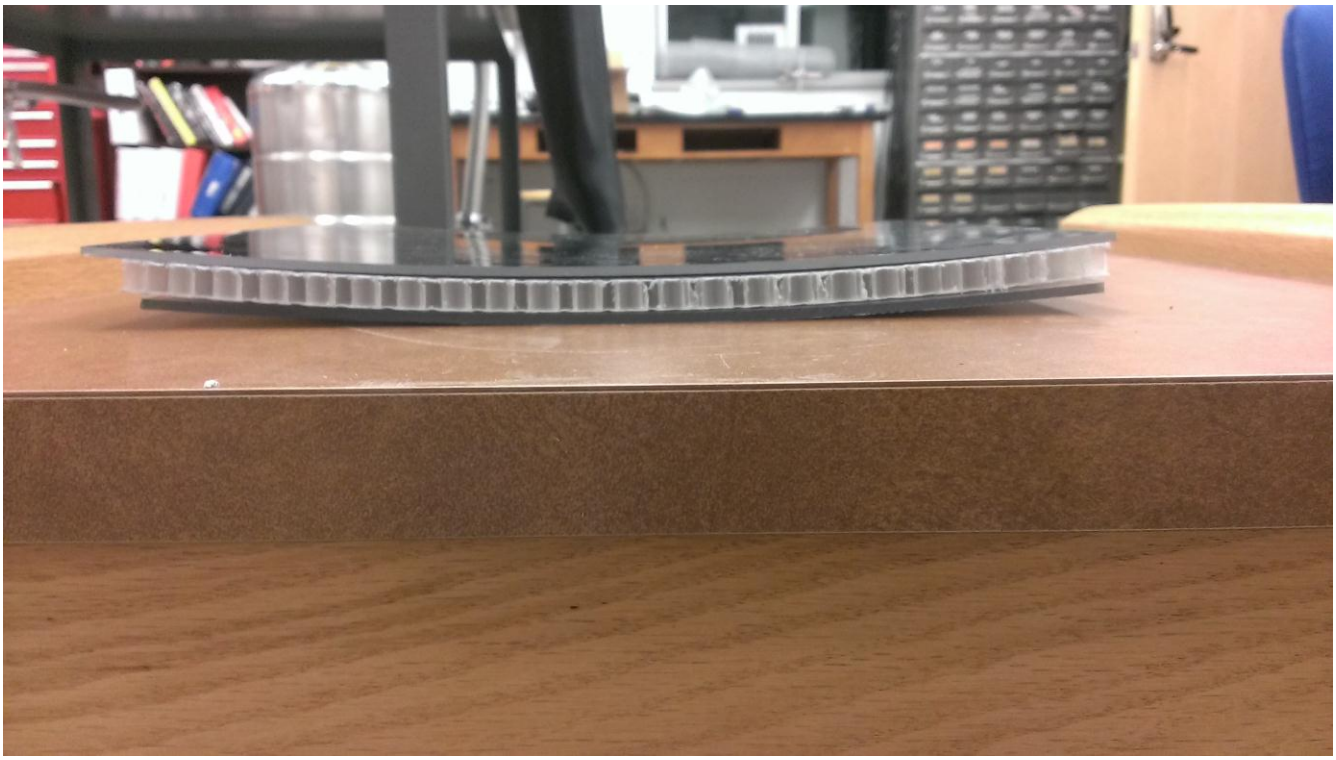

Figure 18: Mirrored Lexan, honeycomb, and clear Lexan that have been shaped using the mould. This is proof of concept for creating a mirror that is supported by honeycomb and a thick Lexan backing.

The three pieces will be epoxied together to make one solid piece. The radius has not been measured yet due to insufficient time to create a smaller frame to hold the pre-curved mirrors.

IV. Goals

This project showed that it is possible to measure the radius of curvature for a mirror using a laser table and a target screen. At this point in time it appears that bending a mirror using pressure will not provide the uniformly curved mirror that is required by GRINCH detector. However, the frame will be crucial for mounting and aligning prefabricated mirrors. The next steps are to measure the radius of curvature for the preformed mirrors and to measure the change in reflectivity of flat mirrors that have been curved.

V. Sources

[1] Averett, Todd D., Huan Yao, and Bogdan Wojtsekhowksi. *GRINCH Detector Technical Document v. 11* *http://wm-jlab.physics.wm.edu/mediawiki/index.php/Bigbite_Gas_Cherenkov* *12/6/2012*

[2] Bletzinger, Kai-Uwe. *Theory of Plates*. Rep. N.p., 2000. Web. 11 Apr. 2013. <http://www.student-info.net/sismapa/skupina_doc/fgg/knjiznica_datoteke/1231148708_zip_vsebina_2del_upogibplosc_teorijainanaliza.pdf>.

[3] Ezeh, J. C., O. M. Ibearugbulem, and C. I. Onyechere. "Pure Bending Analysis of Thin Rectangular Flat Plates Using Ordinary Finite Difference Method." *International Journal of Emerging Technology and Advanced Engineering* 3.3 (2013): 20-23. Web. 5 May 2013. <http://www.ijetae.com/files/Volume3Issue3/IJETAE_0313_04.pdf>.

[4] McLean, Christine. "Design, Testing of a Prototype Heavy Gas Ring-Imaging Cherenkov (GRINCH) Detector." Diss. The College of William and Mary, 2012. *http://wm-jlab.physics.wm.edu/mediawiki/index.php/Bigbite_Gas_Cherenkov 12/6/2012*